OFFICE OF NAVAL RESEARCH

Contract No. N00014-91-J-1409

Technical Report No. 124

Isotopic Ligand Exchange in the High-Nuclearity Platinum Clusters $[Pt_{24}(CO)_{30}]^n$ and $[Pt_{26}(CO)_{32}]^n$ (n=0 to -6) in Dichloromethane: Substitution Kinetics, Carbonyl Dipole Coupling, and Comparisons with Pt(111) Electrodes

by

J.D. Roth, G.J. Lewis, X. Jiang,

L.F. Dahl and M.J. Weaver

Prepared for Publication

in the

Journal of Physical Chemistry

Purdue University

Department of Chemistry

West Lafayette, Indiana 47907

May 1992

ABSTRACT

The effect of substituting ^{12}CO by ^{13}CO on the infrared spectra of $[Pt_{24}(CO)_{30}]^n$ and $[Pt_{26}(CO)_{32}]^n$ (n = 0 to −6) in dichloromethane has been studied in order to explore the nature of the ligand substitution kinetics and dynamic dipole–dipole coupling for these high-nuclearity clusters in relation to metal surfaces. The chargeable nature of the platinum clusters, as scrutinized by FTIR spectroelectrochemical tactics, offers interesting comparisons with the potential-dependent dipole coupling observed for mixed $^{13}CO/^{12}CO$ adlayers at the Pt(111)–dichloromethane interface, also reported here. Unlike the electrochemical surface, CO ligand exchange on $[Pt_{24}(CO)_{30}]^{2-}$ and $[Pt_{26}(CO)_{32}]^{2-}$ is slow and non-random, incomplete $^{12}CO/^{13}CO$ substitution occurring even on long (> several hours) timescales. Substantial deviations from first-order substitution kinetics are also observed, especially for $[Pt_{24}(CO)_{30}]^{2-}$ where only 65% of the CO ligands are observed to undergo exchange. The results suggest the occurrence of a "merry-go-round" ligand migration mechanism from active substitution centers within the monocrystalline Pt facets that make up the cluster surfaces. Consistent with this, the formation of high local ^{13}CO coverages even early in the substitution process is indicated from the strong ^{13}CO dipole coupling, deduced from the terminal C–O stretching frequencies, ν^t_{co}, together with the nonsymmetrical nature of the $^{13}\nu^t_{co}$– and $^{12}\nu^t_{co}$– isotope mole fraction plots. Even though only small CO islands can be formed on the clusters, the ν^t_{co} upshifts due to dynamic dipole–dipole coupling, $\Delta\nu_D$, approach those observed, 30–35 cm^{-1}, for the Pt(111) interface. The magnitude of the dipole–dipole coupling is also dependent on the surface electronic charge for both the clusters and the electrode surface, yet in different ways. For the latter, $\Delta\nu_D$ diminishes markedly as the electrode charge becomes more negative.

There is considerable interest in exploring the physical and chemical properties of high-nuclearity metal clusters, especially in relation to the behavior of related metal surfaces.[1] Notable members of such systems, studied in detail by the Wisconsin group, are the class of platinum carbonyl anions represented by $[Pt_{24}(CO)_{30}]^{2-}$ and $[Pt_{26}(CO)_{32}]^{2-}$. These clusters feature cubic close-packed (ccp) and hexagonal close-packed (hcp) metal cores, respectively, with carbonyl ligands in well-defined terminal and twofold bridging coordination geometries as established by x-ray crystallography.[1-4] Interesting properties exhibited by such clusters are that they are soluble in a range of nonaqueous media, and undergo a sequence of reversible one- (and two-) electron redox transitions to form $[Pt_{24}(CO)_{30}]^n$ and $[Pt_{26}(CO)_{32}]^n$, where n varies between 0 and at least -8.[5,6] The solution-phase clusters are therefore chargeable in a manner closely analogous to metal-solution interfaces, offering the intriguing prospect of exploring the "ionizable metal cluster-electrode surface" analogy.[6]

Furthermore, we have demonstrated recently that infrared spectroelectrochemistry provides a powerful means of examining the charge-dependent structural properties of such metal carbonyl clusters, given the sensitivity of the C-O stretching frequency, ν_{co}, to the carbonyl coordination geometry.[5,6] Such measurements show that the ν_{co} frequencies are sensitive to the cluster charge in a similar fashion to the potential- (and hence charge-) dependent properties of CO adlayers on platinum electrodes. A detailed assessment along these lines has uncovered interesting differences as well as similarities in the potential-dependent spectroelectrochemical behavior of corresponding carbonyl clusters and CO-covered electrodes. These differences are attributable to geometric as well as electronic factors.[6]

Such findings also raise the issue of the manner and extent to which the carbonyl ligand environments may differ in the cluster and interfacial systems.

In the latter case, it is well known that large changes in the ν_{co} frequency are usually induced by increasing the CO surface coverage, θ_{co}. These local adsorbate-adsorbate interaction effects can be separated into dynamic dipole-dipole and "static chemical" contributions by acquiring infrared spectra for differing isotopic mixtures, such as $^{12}CO/^{13}CO$, as a function of θ_{co}.[7] The former effect, in particular, is seen to provide a major component of the large ν_{co} frequency upshifts commonly observed as θ_{co} increases.[7] Although most reported data of this type refer to metal-ultrahigh vacuum (uhv) interfaces, the Purdue group has recently utilized such tactics in exploring environmental effects upon CO adlayer structure at ordered low-index platinum and rhodium electrode surfaces in aqueous media.[8,9]

Analogous ligand-interaction effects can also be envisaged in metal carbonyl clusters. However, while isotopic-substitution tactics have been utilized in small metal clusters, *primarily to* elucidate ligand substitution pathways,[10] essentially no information of this type is available for the higher-nuclearity clusters which are more likely to provide viable models of metal surfaces. We report here infrared spectra for $[Pt_{24}(CO)_{30}]^n$ and $[Pt_{26}(CO)_{32}]^n$ (n = 0 to -6) in dichloromethane, where $^{13}CO/^{12}CO$ isotopic exchange is induced to occur by exposing the ^{12}CO clusters to near-saturated concentrations of ^{13}CO. In contrast to saturated CO adlayers on Pt surfaces, $^{13}CO/^{12}CO$ ligand exchange is observed to be sluggish and, in the case of $[Pt_{24}(CO)_{30}]^n$, incomplete even on long (~1 day) timescales. The observed ligand substitution kinetics, along with the observed infrared spectra for different $^{13}CO/^{12}CO$ ligand ratios, are utilized to deduce the manner of carbonyl exchange and the nature of dipole-dipole coupling for these large metal clusters. Comparisons are made with dipole coupling for saturated CO adlayers at the Pt(111)-dichloromethane interface as extracted from surface infrared spectra for $^{13}CO/^{12}CO$ mixtures.

EXPERIMENTAL

Much of the experimental detail, including the cluster syntheses and the spectroelectrochemical procedures, is outlined elsewhere.[6] The reflectance-type spectroelectrochemical cell employed for the cluster infrared studies is described in detail in ref. 11. It features a micrometer adjustment of the thin-layer thickness (defined by the electrode-surface CaF_2 window separation), and the provision of forced hydrodynamic flow. The latter enables small solution samples, as used here, to efficiently be injected into the thin-layer cavity, via a Pt tube entry through the optical window. The electrode was a 0.9 cm gold disk; this metal was chosen so to avoid spectral interferences from adsorbed CO.

The $^{13}CO/^{12}CO$ ligand exchange for the metal clusters was undertaken in the reactor illustrated in Fig. 1. The cluster-containing solution [in dichloromethane (Fischer) with 0.15 M tetrabutylammonium perchlorate (TBAP)] was injected into the nitrogen-flushed reactor through the top septum. The solution was subjected to two freeze-pump-thaw cycles, and then frozen at liquid nitrogen temperatures. Any noncondensible gases were removed with a vacuum pump. The reactor was then isolated from the pump by closing valve C. The ^{13}CO (99%, Aldrich) was transferred via a metal tube through the top septum, and valve A then closed to prevent leakage through the perforated septum. Since CO is a liquid at 77° K this allowed for a near-quantitative transfer. The 500 ml gas bulb initially contained 4.8 mmoles of ^{13}CO and about 30 mg of cluster (as the tetraphenylarsonium dianion salt). This resulted in approximately a 150 fold excess of ^{13}CO in the reactor. Thus, the back reaction of exchanging ^{12}CO for ^{13}CO is negligible. Aliquots of the solution were transferred into a small reservoir for ensuing spectroelectrochemical examination at various times by opening valve B slightly. After closing valve B, the solution was drawn off with a syringe and placed in small vial which had previously been purged with N_2. The

solution in the arm of the reactor before valve B was then returned to the flask by placing a positive pressure of N_2 in the sampling chamber and opening slightly B. Great care was taken during this procedure to prevent N_2 from being admitted into the reaction chamber. The aliquots were subjected immediately to two freeze-pump-thaw-cycles so to remove solution CO, thereby halting the carbonyl isotopic exchange process, before spectroelectrochemical investigation.

The Pt(111) crystal (9 mm diameter, 4 mm thick) was purchased from the Material Preparation Facility at Cornell University. It was oriented within ±1°, as verified by X-ray diffraction. The surface pretreatment procedure, including hydrogen-air flame annealing, cooling in the presence of iodine vapor, and replacement of the adsorbed iodine with CO in 0.1 M $HClO_4$, has been described previously.[12] The crystal was then thoroughly rinsed with dichloromethane and immediately transferred to the infrared cell, filled with dichloromethane containing 0.15 M TBAP and near-saturated $^{12}CO/^{13}CO$ solution having the desired isotopic ratio. The latter was prepared by mixing ^{13}CO and ^{12}CO-containing dichloromethane in the appropriate ratio. The ^{13}CO solution was prepared similarly to above, and the ^{12}CO solution by bubbling in natural-abundance CO gas (Matheson).

The electrode potentials were measured and are quoted versus the ferrocenium-ferrocene ($Fc^{+/o}$) couple in the same solvent; this involved the use of an equimolar Fc^+/Fc mixture in contact with a Pt wire, contained in a separate compartment. All measurements were made at room temperature, 23±1°C.

RESULTS

Mixed $^{13}CO/^{12}CO$ Adlayers on Pt(111)

While the primary focus here is on the infrared spectral examination of $^{13}CO/^{12}CO$ ligand mixtures in the Pt clusters, as noted above it is of interest to

compare this behavior with that for mixed $^{13}CO/^{12}CO$ adlayers at a closely related platinum electrode interface, Pt(111) in dichloromethane. The latter results will be described first since they provide a basis for assessing the less conventional properties of the Pt clusters.

Typical potential-dependent infrared spectra in the terminal ν_{co} frequency region for a saturated ($\theta_{co} \approx 0.7$) mixed $^{13}CO/^{12}CO$ adlayer on Pt(111) in dichloromethane containing 0.15 M TBAP are shown in Fig. 2A and B, referring to ^{12}CO percentages of 49% and 26%, respectively. [Although a second ν_{co} band at lower frequencies, ca 1780-1860 cm^{-1}, is also obtained,[13] it is markedly weaker and does not yield well-defined spectral features for $^{12}CO/^{13}CO$ mixtures (Fig. 2).[8a]] These spectra were obtained by acquiring sets of 100 interferometer scans (each consuming ca 60s) during a staircase potential ramp from -2.0 V to sequentially more positive potentials, as indicated alongside each spectrum. The solvent and other spectral interferences were removed, as usual,[8] by subtracting a reference spectrum recorded subsequently at a sufficiently positive potential, 1.0 V, so that the CO was removed electrooxidatively. (Although CO electrooxidation to form CO_2 clearly will not occur in rigorously anhydrous dichloromethane, the small amounts of water purposefully present in the solvent enabled this reaction to occur satisfactorily by about 1.0 V.) The proportion of ^{12}CO and ^{13}CO adsorbed on the surface (and present in solution) is determined readily from the ratio of the band intensities appearing in such potential-difference infrared spectra at 2343 and 2275 cm^{-1}, associated with the $^{12}CO_2$ and $^{13}CO_2$ products, respectively, trapped in the spectral thin layer.[8a,14]

The spectra in Fig. 2 display the usual hallmarks of $^{13}CO/^{12}CO$ dipole coupling, especially at higher electrode potentials. Thus substantial "intensity transfer" is observed under these conditions, so that the higher-frequency band partner is markedly more intense relative to the lower-frequency component than

commensurate with the ^{12}CO mole fraction. In addition, the frequencies of both band partners downshift significantly as the ^{12}CO fraction is decreased. This latter feature arises from a progressive diminution in the extent of dipole coupling involving nearby ^{12}CO adsorbate molecules upon dilution with ^{13}CO.

The extent of dipole–dipole coupling within the saturated ^{12}CO adlayer at each potential can be quantified readily by plotting, as usual,[7,8a] the frequencies of the higher- and lower-frequency band partners, $^{12}\nu_{co}$ and $^{13}\nu_{co}$ (associated with ^{12}CO and ^{13}CO, respectively), as a function of the isotopic composition. Figures 3 and 4 show examples of such plots of $^{12}\nu_{co}$ (filled circles) and $^{13}\nu_{co}$ (filled squares) versus $\%^{12}CO$ at electrode potentials of 0.2 and −1.2 V, respectively. The $\%^{12}CO$ ranges over which the $^{12}\nu_{co}$ and $^{13}\nu_{co}$ values are given, $\geq 20\%$ and $\leq 75\%$, respectively, were limited by the ability to discern the peaks in the mixed-isotope spectra. The frequency shift due to dynamic dipole–dipole coupling within the pure ^{12}CO (or ^{13}CO) adlayer, $\Delta\nu_D$, can be found from the difference between the pure-isotope frequency, ^{12}CO (or $^{13}\nu_{co}$), and the $^{12}\nu_{co}$ (or $^{13}\nu_{co}$) value extrapolated to infinite dilution of that isotope at the same total θ_{co}.

Since the use of $^{12}CO/^{13}CO$ mixtures for adlayer dosing necessarily creates a random distribution of isotopes on the surface, we expect that[7]

$$\Delta^{12}\nu_{co}(^{12}x_1 \rightarrow {}^{12}x_2) = \Delta^{13}\nu_{co}(^{13}x_1 \rightarrow {}^{13}x_2) \qquad (1)$$

where $\Delta^{12}\nu_{co}$ is the shift of the high-frequency peak caused by altering the mole fraction of ^{12}CO from x_1 to x_2, and $\Delta^{13}\nu_{co}$ is the low-frequency peak shift caused by the same alteration of the mole fraction in ^{13}CO. In other words, the $^{12}\nu_{co} - {}^{12}x$ and $^{13}\nu_{co} - {}^{13}x$ plots should be mirror images to each other. As an illustration, the open triangles in Figs. 3 and 4 are estimates of the $^{13}\nu_{co} - {}^{13}x$ plot obtained from the corresponding $^{12}\nu_{co} - {}^{12}x$ data by using Eq(1), and assuming

that the ν^t_{co} difference for the pure ^{12}CO and ^{13}CO adlayers is determined by the reduced masses (ca 45 cm^{-1}). These estimated $^{13}\nu_{co} - {}^{13}x$ points are seen to be close to the actual $^{13}\nu_{co} - {}^{13}x$ data (squares); the residual discrepancies are due partly to slight deviations in ($^{12}\nu_{co} - {}^{13}\nu_{co}$) from the frequency shifts based on reduced masses.[8a] The use of Eq(1) to examine the non-random distribution of $^{12}CO/^{13}CO$ isotopes within dipole-coupled ligand arrays for the Pt clusters is pursued below.

The present dipole-coupling data for Pt(111)/CO in dichloromethane are similar to those reported earlier for saturated CO adlayers at the Pt(111)-aqueous interface.[8a] The latter refer to the more restricted potential range from -0.25 to 0.2 V vs the saturated calomel electrode, SCE (equivalent to ca -0.45 to 0 V vs $Fc^{+/o}$). Sequential, rather than concurrent, surface dosing with ^{13}CO and ^{12}CO yielded near-complete isotopic replacement within ca 10 min., indicating that the ligand-exchange processes is rapid in the presence of solution CO. Mixed $^{12}CO/^{13}CO$ adlayers formed by such sequential dosing yielded essentially identical dipole coupling features to those formed by concurrent dosing, indicating that randomly distributed isotopic mixtures are formed under these conditions.[8b]

One other, more unexpected, feature of the present results for Pt(111)/CO is that the extent of dipole-dipole coupling depends noticeably on the electrode potential, the coupling tending to diminish towards more negative potentials. This can be discerned most easily from the spectra in Fig. 2, in that the extent of intensity transfer towards the higher-frequency band partner decreases markedly as the potential becomes more negative. More pointedly, the frequency upshift due to dipole coupling, $\Delta\nu_D$, also diminishes under these conditions. As a semiquantitative illustration, Fig. 5 is a plot of the shift in the higher-frequency band partner, $\Delta^{12}\nu_{co}$, between 27% and 100% ^{12}CO as a function of the

electrode potential, E. While the plot exhibits some scatter, $\Delta^{12}\nu_{co}$ clearly decreases monotonically for potentials negative of ca −0.5 to 0 V. Interestingly, the ^{12}CO adlayer structure on Pt(111) is known to undergo a structural change at about −0.3 V vs $Fc^{+/o}$ (ca 0 V vs SCE), as discerned from a change in the ν^{t}_{co} − E slope and a marked alteration in the frequency of the bridging ν_{co} feature.[13] The terminal band intensity for the pure ^{12}CO adlayer remains essentially constant over the potential range −0.5 to −2.0 V where $\Delta^{13}\nu_{co}$ diminishes, thereby indicating that the potential-dependent dipole coupling is unlikely to be due to variations in the CO coverage.

$^{13}CO/^{12}CO$ Exchange in $[Pt_{24}(CO)_{30}]^{n}$ and $[Pt_{26}(CO)_{32}]^{n}$

Since the metal clusters examined here are synthesized as pure ^{12}CO carbonyls, in order to examine dipole coupling effects it is necessary to partially replace the ^{12}CO ligands with ^{13}CO by isotopic exchange. As noted in the Experimental Section, a ca 0.4 mM solution of each cluster in dichloromethane was exposed to a 150 fold excess of dissolved ^{13}CO, aliquots being removed for spectroelectrochemical examination at various time intervals. Since the ^{13}CO is in large excess, virtually complete replacement of ^{12}CO ligands by ^{13}CO should occur. However, the kinetics of ligand exchange for both $[Pt_{24}(CO)_{30}]^{2-}$ and $[Pt_{26}(CO)_{32}]^{2-}$ turn out to be sufficiently sluggish so that only partial isotopic exchange occurs even on long (> several hours) timescales. The fraction of ^{12}CO ligand remaining on the clusters after a given ^{13}CO exposure time, t_{13}, was determined from the ratio of the $^{12}CO_2$ to $^{13}CO_2$ band intensities (at 2343 and 2275 cm^{-1}, respectively), obtained by electrooxidizing entirely the cluster ligands at the gold electrode at an appropriately high potential, ca 1.0 V. [This tactic is similar to that used to assay mixed isotopic adlayers on Pt(111) as noted above. One difference, however, is that uncoordinated (solution-phase)

CO is absent during the cluster spectroelectrochemistry, so that the ligand composition should faithfully be determined.]

These experiments enable the rate of ^{12}CO ligand substitution by ^{13}CO to be examined as a function of the isotopic carbonyl composition. In the simplest (albeit unexpected) case where each of the carbonyl coordination sites in the cluster are equivalent, the isotopic substitution kinetics will be first order with respect to $\%^{12}CO$, in which case we will obtain a linear plot of log ($\%^{12}CO$) versus t_{13}, where $\%^{12}CO$ is the percentage of ^{12}CO ligand surviving in the clusters at a given reaction time t_{13}. Figure 6 shows such first-order plots (filled circles) for $[Pt_{24}(CO)_{30}]^{2-}$ (A) and $[Pt_{26}(CO)_{32}]^{2-}$ (B). The former plot is clearly nonlinear, the isotopic substitution essentially ceasing (over ca 1½ days) when $\%^{12}CO$ declines to 35% (Fig. 6A). Nevertheless, the substitution kinetics prior to this point are approximately first order, as can be seen by replotting only the "replaceable" portion of ^{12}CO, i.e., log ($\%^{12}CO$ - 35%) vs t_{13} (open circles in Fig. 6A). The slope of this initial region yields a half life, $t_{\frac{1}{2}}$, of ca 90 min. Somewhat different behavior was observed for $[Pt_{26}(CO)_{32}]^{2-}$ (Fig. 6B). While the first ca 15% of the ^{12}CO replacement occurred very rapidly ($\lesssim$ 10 min.), the remaining substitution yielded roughly uniform first-order kinetics, with $t_{\frac{1}{2}} \approx 250$ min.

Given these deviations from pure first-order kinetics, the substitution process is expected to yield non-random $^{12}CO/^{13}CO$ mixing on the cluster surfaces. Evidence that this is indeed the case is obtained by examining the cluster ν_{CO} infrared spectra as a function of $\%^{12}CO$. Figure 7 shows illustrative spectra for $[Pt_{24}(CO)_{30}]^{n}$ (n = -2 to -6, as indicated) for a pair of $\%^{12}CO$ values, 50% (A) and 35% (B). The spectra for the consecutive reduced states (-n > 2) were obtained by sweeping the electrode potential negative at 5 mV s^{-1} so to sequentially reduce $[Pt_{24}(CO)_{30}]^{2-}$ in one-electron steps. The bottom spectrum in Figs. 7A and

B was obtained after reoxidizing the cluster to the dianion form.

Two significant features of these spectra are immediately evident. First, the form of the mixed isotope spectra in the terminal ν_{co} region (ca 1900–2050 cm^{-1}) change substantially as the cluster is reduced. For $-n \leq 4$, a pair of distinct ν_{co} bands are obtained that appear roughly similar to those observed for CO adlayers (Fig. 2). The ca 15 cm^{-1} ν_{co} frequency downshifts seen here upon one-electron reduction are close to those observed for the single terminal band in the pure ^{12}CO spectra (see Fig. 2 in ref. 5). For more highly reduced clusters ($n = -5,-6$), however, the band becomes broader and the higher-frequency (^{12}CO) partner merges into the lower-frequency component. This finding is indicative of a charge-induced alteration in the carbonyl environment. The changes are largely reversed, however, upon reoxidizing the cluster to $n = -2$ (Fig. 7). Second, for $-n \leq 4$ there is a substantial difference in the relative intensities of the higher- and lower-frequency band partners between Figs. 7A and B, even though $\%^{12}CO$ drops only from 50 to 35%. While the former spectra indicates the presence of marked intensity transfer, such an effect is virtually absent in the latter spectra in that the relative intensities of the high- and low-frequency band partners (~1:2) matches closely the ^{12}CO:^{13}CO ligand ratio.

A non-random nature of the progressive ^{12}CO – ^{13}CO substitution on $[Pt_{24}(CO)_{30}]^n$ is indicated further from plots of $^{12}\nu_{co}$ (circles) and $^{13}\nu_{co}$ (squares) versus $\%^{12}CO$ for $[Pt_{24}(CO)_{30}]^n$; examples are given for $n = -1$ and -3 in Figs. 8 and 9, respectively. As for the analogous data for $^{12}CO/^{13}CO$ adlayers on Pt(111) (Figs. 3,4), included in Figs. 8 and 9 are $^{13}\nu_{co}$ – $\%^{12}CO$ points (triangles, dashed trace) estimated from the corresponding $^{12}\nu_{co}$ – $\%^{12}CO$ data by means of Eq(1) as outlined above. Unlike the Pt(111)/CO adlayers, these observed and estimated $^{13}\nu_{co}$ – $\%^{12}CO$ plots for the Pt carbonyl clusters are distinctly divergent, especially towards higher $\%^{12}CO$ (Figs. 8,9). Most notably, while $^{12}\nu_{co}$ downshifts

quite markedly as $\%^{12}CO$ decreases, especially for $\%^{12}CO \lesssim 50\%$, $^{13}\nu_{co}$ exhibits much smaller changes than anticipated from Eq(1) on this basis.

These findings suggest that while the extent of dipole coupling experienced by the ^{12}CO ligands diminishes markedly as $\%^{12}CO$ decreases, that for the incoming ^{13}CO ligands remains more invariant as isotopic substitution proceeds. Moreover, even at high $\%^{12}CO$ values, $\gtrsim 80\%$, the frequency differences ($^{12}\nu_{co} - {}^{13}\nu_{co}$) in Figs. 8 and 9 are comparable to those, ca 45 cm^{-1}, expected in the absence of dipole coupling (i.e., that arising merely from the difference in the ^{12}CO and ^{13}CO reduced masses), and markedly smaller than those anticipated from Eq(1). Provided that significant dipole coupling is indeed present in the pure ^{12}CO (and ^{13}CO) ligated clusters, this result indicates that the ^{13}CO ligands experience a substantial fraction of the coupling *even* at early stages of the substitution process.

Roughly comparable results were also obtained for $[Pt_{26}(CO)_{32}]^n$. Displayed in Figs. 10A and B are infrared spectra from n = 0 to −6 for 64% and 49% ^{12}CO, respectively. (Note that the n = −3 and −5 states for $[Pt_{26}(CO)_{32}]^n$ are inaccessible in dichloromethane, direct two-electron reductions from the n = −2 and −4 states being observed instead.[6]) Plots of $^{12}\nu_{co}$ (circles) and $^{13}\nu_{co}$ (squares) versus $\%^{12}CO$ for the n = −1 and −4 forms of $[Pt_{26}(CO)_{32}]^n$ are given in Figs. 11 and 12, respectively. Similarly to figs. 8 and 9 for $[Pt_{24}(CO)_{30}]^n$, the $^{12}\nu_{co}$ downshifts induced as $\%^{12}CO$ decreases are not mirrored by complimentary changes in $^{13}\nu_{co}$. Indeed, $^{13}\nu_{co}$ tends to *downshift* slightly as $\%^{12}CO$ decreases, rather than increase in the manner predicted by Eq(1) (as before, plotted as triangles in Figs. 11 and 12). Again, the ($^{12}\nu_{co} - {}^{13}\nu_{co}$) differences are relatively small, ca 40–45 cm^{-1}, even at high $\%^{12}CO$ values ($\gtrsim 70\%$), indicating that comparable amounts of dipole coupling are experienced by ^{13}CO even in the initial stages of isotopic replacement, where $\%^{13}CO \ll \%^{12}CO$. Evidently, then,

^{12}CO substitution by ^{13}CO occurs in a decidedly non-random fashion also for $[Pt_{26}(CO)_{32}]^n$.

The quantitative evaluation of the terminal band frequency upshift due to dipole coupling, $\Delta\nu_D$, is impeded by the non-random nature of the $^{13}CO/^{12}CO$ substitution process, together with the difficulty of achieving near-complete ^{12}CO substitution. Nevertheless, the $\Delta\nu_D$ values appear to be at least 15–20 cm^{-1} for both $[Pt_{24}(CO)_{30}]^n$ and $[Pt_{26}(CO)_{32}]^n$ on the basis of the $^{12}\nu_{co}$ downshifts observed upon ^{12}CO replacement ("dilution") by ^{13}CO. In addition, $\Delta\nu_D$ appears to increase significantly as -n becomes larger, more clearly for $[Pt_{26}(CO)_{32}]^n$. For example, the $\Delta^{12}\nu_{co}$ value resulting from diminishing $\%^{12}CO$ from 100 to 30% increases from 17 cm^{-1} for n = 0 to 28 cm^{-1} for n = -6. This apparent enhancement in the extent of dipole coupling is in harmony with the greater intensity transfer observed under these conditions, as noted above.

DISCUSSION

The marked deviations from first-order kinetics for $^{13}CO/^{12}CO$ replacement in $[Pt_{26}(CO)_{32}]^{2-}$ and especially in $[Pt_{24}(CO)_{30}]^{2-}$, together with the asymmetric nature of the $^{12}\nu_{co}$ - $\%^{12}CO$ and $^{13}\nu_{co}$ - $\%^{13}CO$ plots provide clear evidence that the ligand substitution process is highly non-random. That is, carbonyl substitution occurs preferentially at particular coordination sites on the cluster. Qualitatively similar observations have been made on several occasions for smaller carbonyl clusters.[10,15] Given that the CO ligands on metal carbonyls are usually found to be fluxional,[16,17] isotopic substitution can be envisaged to involve carbonyl migration from preferred exchange sites, hence dispersing ^{13}CO to other positions on the metal core.

Such an "active site-migration" mechanism predicts that the invading ^{13}CO will form "islands", rows, or rings around the metal core. These contiguous

isotopic distributions should exhibit significant $^{13}\nu_{co}$ upshifts due to dipole coupling even at low ^{13}%CO, which are relatively invariant as ^{13}%CO increases. The similarity of this predicted behavior with the observations for both $[Pt_{24}(CO)_{30}]^n$ (Figs. 7,8) and $[Pt_{26}(CO)_{32}]^n$ (Figs. 10,11) by itself provides strong evidence that such ^{13}CO aggregations are being formed even at an early stage of the ligand replacement process.

Some insight into the likely migration mechanisms for the present high-nuclearity systems can be provided from earlier studies on smaller carbonyl clusters.[16-18] Carbonyl ligand migration is known to be a multi-centered process which probably occurs through bridging intermediates. For a terminal CO ligand to move to a terminal position on an adjacent metal atom it apparently must first move into the bridging site common to both metal atoms. This often involves the movement of several CO ligands in unison. A classic example of this, the "merry-go-round" mechanism,[16] is shown in Fig. 13. There also appears to be a three-dimensional form of this process where the ligands which undergo a facile interchange share a common conical surface above a polyhedral face. It is suspected that this type of mechanism may be important for large metal carbonyl clusters.[16]

Both $[Pt_{24}(CO)_{30}]^n$ and the $[Pt_{26}(CO)_{32}]^n$ contain multiple conical surfaces which may have the ability to support three-dimensional merry-go-round ligand-migration processes. The core of each of the clusters can be thought of as layers of Pt atoms. The $[Pt_{24}(CO)_{30}]^{2-}$ cluster (see Fig. 14) consists of two rows of two Pt atoms (first layer) centered above three rows of three Pt atoms (second layer), which in turn are above two rows of four Pt atoms (third layer) and one row of three Pt atoms (fourth layer). The first, second, and third layers of this core are conic sections which contain a polyhedral face. Several other conic sections, at angles to the three already mentioned, provide further

possible pathways for ligand migration.

Consequently, on this basis the invading ^{13}CO ligands may be predicted to gain access to the entire cluster even if only a small fraction of the carbonyl coordination sites engage in ligand exchange. However, this is clearly not the case since only 65% of the CO ligands in $[Pt_{24}(CO)_{30}]^{2-}$ are observed to undergo isotopic exchange, indicating that some of the possible migration pathways are greatly impeded. The precise identity of the 10(±1) remaining (i.e., non-exchanging) ^{12}CO ligands within the cluster structure (Fig. 14) is unclear. However, at least the terminally bound surviving ^{12}CO members appear to be largely isolated, that is surrounded largely by ^{13}CO ligands, judging by the substantial (10-20 cm^{-1}) $^{12}\nu_{CO}$ downshifts observed as $\%^{12}CO$ approaches 35% (Figs. 8,9). This finding is consistent with the formation of ^{13}CO rings around the metal core via a merry-go-round process since these loops would tend to fractionate the remaining ^{12}CO ligands.

The core of the $[Pt_{26}(CO)_{32}]^{2-}$ cluster (see Fig. 15) can be regarded as a plane of 12 Pt atoms sandwiched in between two 7 atom Pt planes. All three of these layers are conic sections which contain a polyhedral face that could support three-dimensional merry-go-round ligand migration. Several other conic sections at 90° to the three already mentioned could also provide such migration. A significant difference compared with $[Pt_{24}(CO)_{30}]^{2-}$ is that ^{13}CO substitution in $[Pt_{26}(CO)_{32}]^{2-}$ proceeds largely to completion in a largely first-order fashion (Fig. 6). This infers that the invading ^{13}CO ligands gain access to most carbonyl coordination sites with comparable facility. A rationalization of the more uniform ligand accessibility of $[Pt_{26}(CO)_{32}]^{2-}$ versus $[Pt_{24}(CO)_{30}]^{2-}$ is that the former cluster features less "sharp edges" than the latter; such facet corners may impede the concerted ligand migration process.

Further support for the "active site-migration" mechanism for carbonyl

exchange is found from the initially rapid substitution kinetics observed for $[Pt_{26}(CO)_{32}]^{2-}$, the first ca 15% being displaced by ^{13}CO with markedly greater facility than the remaining ^{12}CO ligands (Fig. 6B). This observation suggests that five or so CO ligands can be substituted directly with solution ^{13}CO, the remaining carbonyls being displaced more slowly by means of ligand migration from these active centers. A similar situation may apply also to $[Pt_{24}(CO)_{30}]^{2-}$, even though no initially "more rapid" components of the substitution kinetics are observed. The rates, and hence timescales, of direct $^{13}CO/^{12}CO$ replacement and ligand migration could be insufficiently different to be resolvable in this case.

As noted above, it is of interest to compare environmental effects upon the carbonyl ligand properties in the Pt cluster and interfacial electrochemical systems as revealed by $^{12}CO/^{13}CO$ exchange. The present results uncover several significant and even notable dissimilarities, some (but not all) of which can be understood in terms of the structural differences between these two system types. The relatively rapid and essentially random $^{12}CO/^{13}CO$ exchange that occurs at Pt(111) electrochemical interfaces presumably arises from the lower fractional coverages (0.6–0.7 CO's per surface Pt atom[8]) compared with the Pt clusters (ca 1.3),together with the presence of adsorbed CO in twofold bridging as terminal coordination sites,[8a] thereby facilitating exchange between solution and adsorbed CO and adsorbate migration. A limitation in the latter has, nonetheless, been observed in that islands of ^{12}CO and ^{13}CO formed at the Pt(111)–aqueous interface by dosing the former onto adlayer islands of the latter formed by partial electrooxidation remain largely segregated.[8b] The markedly more sluggish as well as non-random nature of $^{13}CO/^{12}CO$ exchange on the Pt clusters compared with Pt(111) (and other Pt surfaces) presumably reflects in part the "tighter" packing of the carbonyl ligands around the Pt cores.

A notable feature of the present Pt clusters is that the carbonyl ligands

experience degrees of dynamic dipole–dipole coupling, $\Delta\nu_D$, which appear to approach those (ca 30–35 cm^{-1}) observed for saturated CO adlayers on Pt(111).[8a] This finding is perhaps surprising given that arrays of parallel CO dipoles are often considered to be necessary for the occurrence of such strong dipole coupling.[7a] Only pairs, or at most quartets, of such parallel CO ligands are present in the Pt clusters (Figs. 14,15), although some coupling could also be anticipated between nearby non-parallel dipoles given the cosine angular dependence predicted from simple theory.[7a] Nevertheless, there are reasons to believe that the nature of the dipole coupling in the clusters is distinct from that operable within the CO adlayers.

One manifestation of such differences is to be found in the electrode potential- (or charge-) dependence of the coupling. While the degree of dipole coupling for the Pt(111)/CO adlayer, as reflected in the degree of intensity transfer as well as in $\Delta\nu_D$, diminishes as the electrode potential (and also the electrode charge[13]) becomes more negative (Figs. 2,5), the opposite effect is found for Pt clusters having progressively more negative charges (Figs. 7,10). Interpretation of these differences, however, is not straightforward since our theoretical understanding of dynamic dipole coupling is very incomplete[7a] and the effects of external electric fields as are present in both the charged surface and cluster systems have apparently not yet been included in these treatments. It is worth noting in this context that the negative charge densities (expressed in terms of excess electronic charge per surface Pt atom) are substantially larger for the present Pt clusters (with $n = -4,-6$) than encountered for Pt(111) even at relatively negative potentials, say −1 to −2 V vs $Fc^{+/o}$.[6] Consequently, then, the local electrostatic fields as well as stereochemical surroundings experienced by the CO ligands in the high-nuclearity Pt clusters can be quite different to those for CO adlayers on Pt surfaces.

In conclusion, the present examination of $^{13}CO/^{12}CO$ isotopic substitution within $[Pt_{24}(CO)_{30}]^n$ and $[Pt_{26}(CO)_{32}]^n$ has uncovered substantial differences in the environmental properties of the carbonyl ligands as compared with close-packed CO adlayers on ordered Pt surfaces. The observed differences, most notably in the kinetics and mechanism of isotopic CO substitution, are understandable qualitatively in terms of the microscopic facetted character of the cluster surfaces. Despite the differences, the extent of CO dipole coupling on the clusters bears an interesting resemblance to that observed for planar CO adlayers. Combined with the close similarities between the electronic charge-dependent ν_{CO} frequencies on the Pt clusters and Pt electrodes, there is good reason to pursue further such "ionizable metal cluster-electrode surface" analogies.[6] Besides yielding further insight into the degree to which the properties of charge clusters converge into those of metal surfaces, such studies should portend a significant merging of understanding in cluster chemistry and surface electrochemistry.

ACKNOWLEDGMENTS

This work is supported by the Office of Naval Research (to MJW) and by the National Science Foundation, via Grants CHE-88-18345 (to MJW) and CHE-86-16697 (to LFD). We are indebted to Johnson-Matthey Inc., Metal Loan Programs (West Deptford, NJ) for supplying a sample of chloroplatinic acid, from which some of the platinum carbonyl clusters were prepared.

REFERENCES AND NOTES

1. For a recent review, see: Kharas, K.C.C.; Dahl, L.F., Adv. Chem. Phys., Prigogini, I, Rice, S.A., eds, Wiley, New York, 1988, Vol. 70, Part 2, p.1

2. Washecheck, D.M., Ph.D. dissertation, University of Wisconsin-Madison, 1980

3. Montag, R.A.; Ceriotti, A.; Dahl, L.F., unpublished results

4. Lewis, G.J., Ph.D. dissertation, University of Wisconsin-Madison, 1991

5. Lewis, G.J.; Roth, J.D.; Montag, R.A.; Safford, L.K.; Gao, X.; Chang, S.-C.; Dahl, L.F.; Weaver, M.J., J. Am. Chem. Soc., 1990, 112, 2831

6. Roth, J.D.; Lewis, G.J.; Safford, L.K.; Jiang, X.; Dahl, L.F.; Weaver, M.J., J. Am. Chem. Soc., submitted

7. For explanative discussions, see: (a) Hollins, P.; Pritchard, J., Prog. Surf. Sci., 1985, 19, 275; (b) Hayden, B.E., in "Vibrational Spectroscopy of Molecules on Surfaces", Yates, Jr., J.T.; Madey, T.E., eds, Plenum, New York, 1987, Chapter 7; (c) Hoffman, F.M., Surf. Sci. Rep., 1983, 3, 107

8. (a) Chang, S.-C.; Weaver, M.J., J. Chem. Phys., 1990, 92, 4582; (b) Chang, S.-C.; Roth, J.D.; Weaver, M.J., Surface Sci., 1991, 244, 113

9. For an overview, see: Chang, S.-C.; Weaver, M.J., J. Phys. Chem., 1991, 95, 5391

10. For a recent review, see: Darensbourg, D.J., in "The Chemistry of Metal Cluster Complexes", Shriver, D.F.; Kaesz, H.D.; Adams, R.D., VCH Publishers, New York, 1990, Chapter 4

11. Roth, J.D.; Weaver, M.J., J. Electroanal. Chem., 1991, 307, 119

12. Leung, L.-W.H.; Wieckowski, A.; Weaver, M.J., J. Phys. Chem., 1988, 92, 6985

13. Chang, S.-C.; Jiang, X.; Roth, J.D.; Weaver, M.J., J. Phys. Chem., 1991, 95, 5378

14. This procedure includes a correction for the small differences in the $^{12}CO_2$ and $^{13}CO_2$ infrared band absorptivities.[8a]

15. Nomiya, K.; Suzuki, H., J. Organomet. Chem., 1979, 168, 115

16. Band, E.; Muetterties, E.L., Chem. Rev., 1978, 78, 639

17. Mingos, D.M.P.; Wales, D.J., "Introduction to Cluster Chemistry", Prentice Hall, Englewood Cliffs, NJ, 1990, Chapter 6

18. (a) Mingos, D.M., Chem. Soc. Rev., 1986, 15, 31; (b) Adams, R.D.; Horvath, I.T., Prog. Inorg. Chem., 1985, 33, 127; (c) Benfield, R.E.; Johnson, B.F.G., Transition Met. Chem., 1981, 6, 131; (d) Horwitz, C.P.; Shriver, D.F., Adv. Organomet. Chem., 1984, 23, 219

FIGURE CAPTIONS

Fig. 1

Diagram of the reactor used to expose the Pt clusters to ^{13}CO in dichloromethane

Fig. 2

Potential-dependent infrared spectra for saturated mixed $^{13}CO/^{12}CO$ adlayers on ordered Pt(111) in dichloromethane containing 0.15 M TBAP, for (A) 49% ^{12}CO and (B) 26% ^{12}CO. Potentials indicated are versus ferrocenium-ferrocene ($Fc^{+/o}$) reference electrode. See text for procedural details.

Fig. 3

Plot of frequencies of higher- and lower-frequency band components, $^{12}\nu_{co}$ (filled circles) and $^{13}\nu_{co}$ (filled squares), versus $\%^{12}CO$ saturated mixed $^{12}CO/^{13}CO$ adlayer on Pt(111) in dichloromethane containing 0.15 M TBAP. Electrode potential is 0.2 V vs $Fc^{+/o}$. Open triangles are $^{13}\nu_{co}$ values estimated from $^{12}\nu_{co}$ - $\%^{12}CO$ data by using Eq(1) as outlined in the text.

Fig. 4

As for Fig. 3, but at electrode potential of -1.2 V vs $Fc^{+/o}$

Fig. 5

Shift in higher-frequency band partner, $\Delta^{12}\nu_{co}$, between 27% and 100% ^{12}CO for saturated $^{13}CO/^{12}CO$ adlayer on Pt(111) in dichloromethane versus the electrode potential (vs $Fc^{+/o}$)

Fig. 6

First-order plots of percentage ^{12}CO (logarithmic scale) remaining on (A) $[Pt_{24}(CO)_{30}]^{2-}$ (filled circles), and (B) $[Pt_{26}(CO)_{32}]^{2-}$ (filled triangles) versus time of exposure (min.) to ^{13}CO in dichloromethane. The open circles in A are the $\%^{12}CO$ values minus 35%; i.e., with the slow-exchanging portion subtracted out (see text for details).

Fig. 7

Infrared spectra of $[Pt_{24}(CO)_{30}]^{n}$ in dichloromethane containing 0.15 M TBAP as a function of the charge, n, as indicated, for cluster containing (A) 48% and (B) 35% ^{12}CO. The mixed $^{12}CO/^{13}CO$ clusters were prepared as noted in the text, involving prior exposure of $[Pt_{24}(CO)_{30}]^{2-}$ to ^{13}CO in dichloromethane for (A) 162 min. and (B) 1855 min.

Fig. 8

As in Fig. 3, but for $[Pt_{24}(CO)_{30}]^{-}$ containing various $\%^{12}CO$ following progressive replacement of ^{12}CO in $[Pt_{24}(CO)_{30}]^{2-}$ by exposure to ^{13}CO in dichloro-

methane. Data refer to $[Pt_{24}(CO)_{30}]^-$ in dichloromethane containing 0.15 M TBAP, formed by electrooxidation of $[Pt_{24}(CO)_{30}]^{2-}$ in spectroelectrochemical cell following removal of aliquots from ^{13}CO reactor (see text for further details).

Fig. 9

As for Fig. 8, but for $[Pt_{24}(CO)_{30}]^{3-}$

Fig. 10

Infrared spectra of $[Pt_{26}(CO)_{32}]^n$ in dichloromethane containing 0.15 M TBAP as a function of the charge, n, as indicated, for cluster containing (A) 64% and (B) 49% ^{12}CO. The mixed $^{12}CO/^{13}CO$ clusters were prepared as noted in the text, involving prior exposure of $[Pt_{26}(CO)_{32}]^{2-}$ to ^{13}CO in dichloromethane for (A) 105 min. and (B) 275 min.

Fig. 11

As in Fig. 3, but for $[Pt_{26}(CO)_{32}]^-$ containing various $\%^{12}CO$ following progressive replacement of ^{12}CO in $[Pt_{26}(CO)_{32}]^{2-}$ by exposure to ^{13}CO in dichloromethane. Data refer to $[Pt_{26}(CO)_{32}]^-$ in dichloromethane containing 0.15 M TBAP, formed by electrooxidation of $[Pt_{26}(CO)_{32}]^{2-}$ in spectroelectrochemical cell following removal of aliquots from ^{13}CO reactor (see text for further details).

Fig. 12

As for Fig. 11, but for $[Pt_{26}(CO)_{32}]^{4-}$

Fig. 13

Schematic "merry-go-round" ligand migration process for triatomic metal cluster (after ref. 16)

Fig. 14

ORTEP for $[Pt_{24}(CO)_{30}]^{2-}$

Fig. 15

ORTEP for $[Pt_{26}(CO)_{32}]^{2-}$

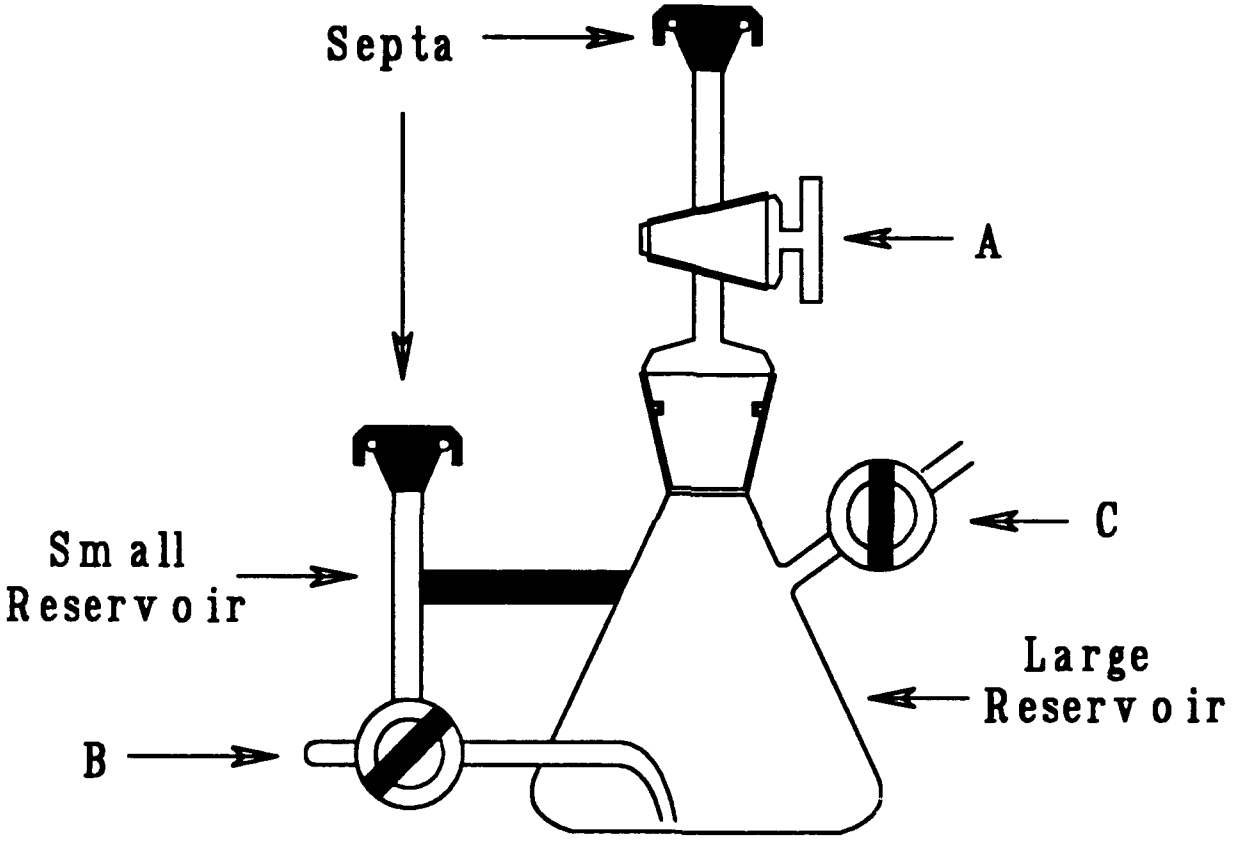

FIG 1

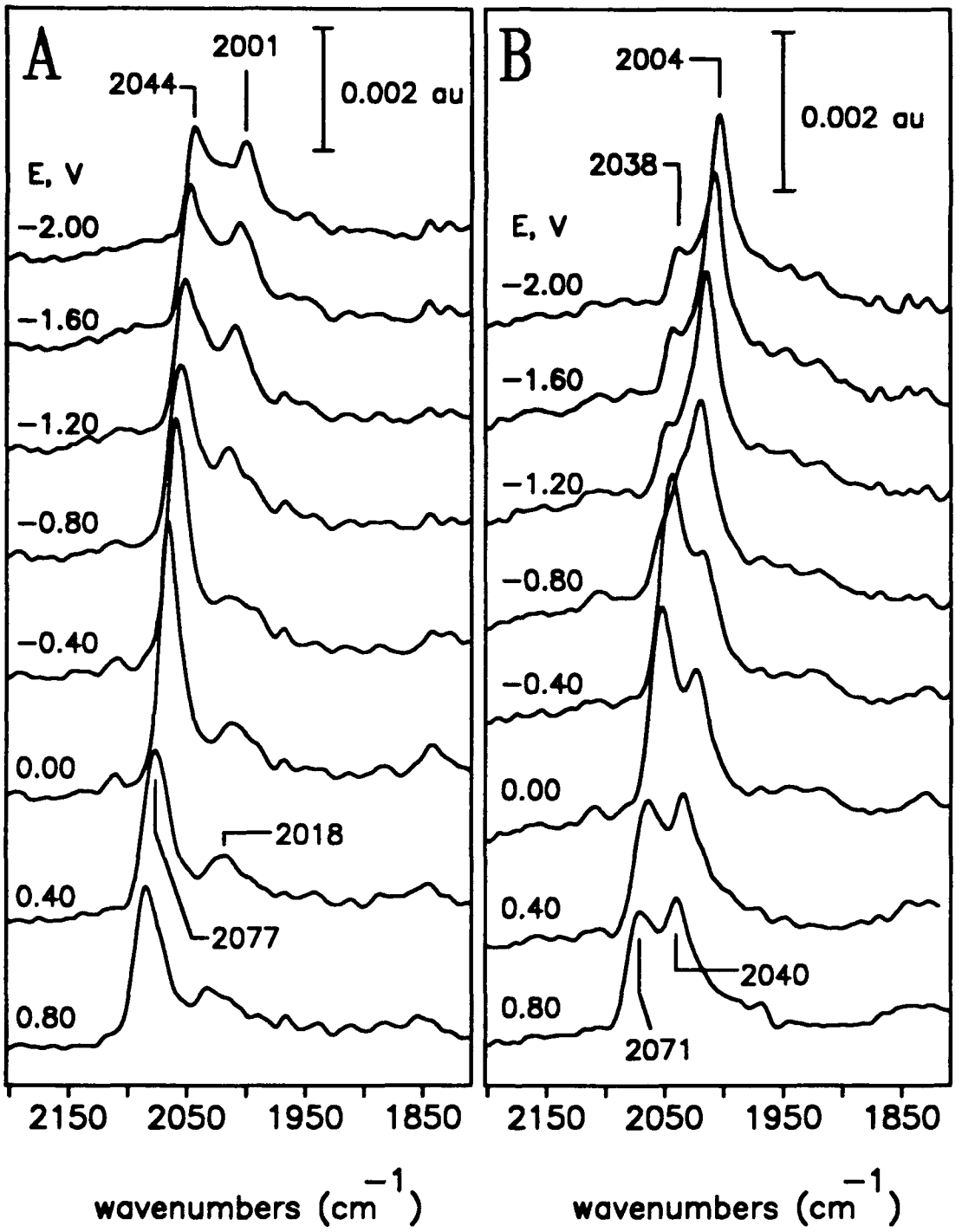
A
2044
2001
0.002 au
E, V
−2.00
−1.60
−1.20
−0.80
−0.40
0.00
0.40
0.80
2018
2077
2150
2050
1950
1850
wavenumbers (cm−1)
B
2004
0.002 au
2038
E, V
−2.00
−1.60
−1.20
−0.80
−0.40
0.00
0.40
0.80
2040
2071
2150
2050
1950
1850
wavenumbers (cm−1)

FIG 2

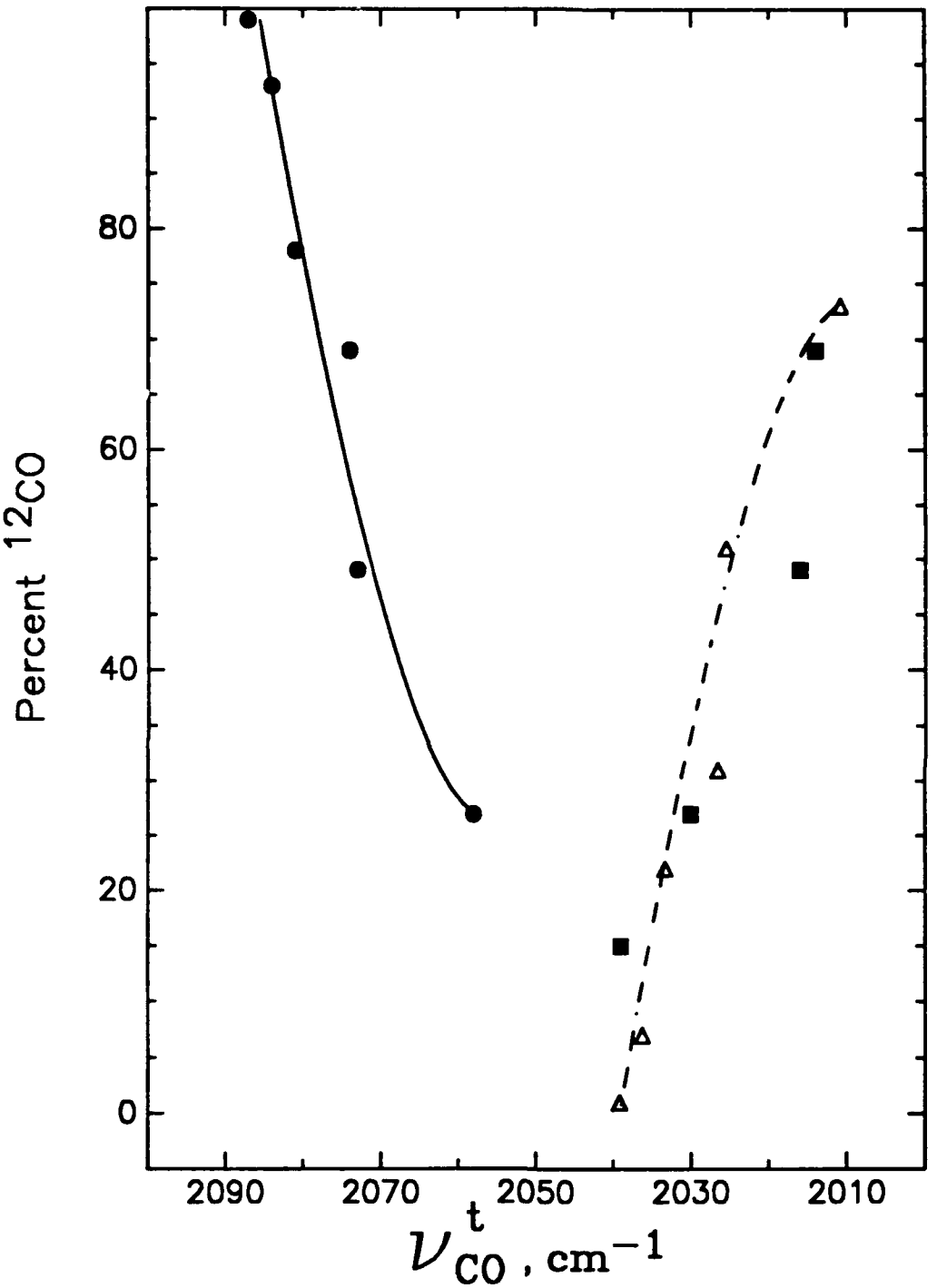

FIG 3

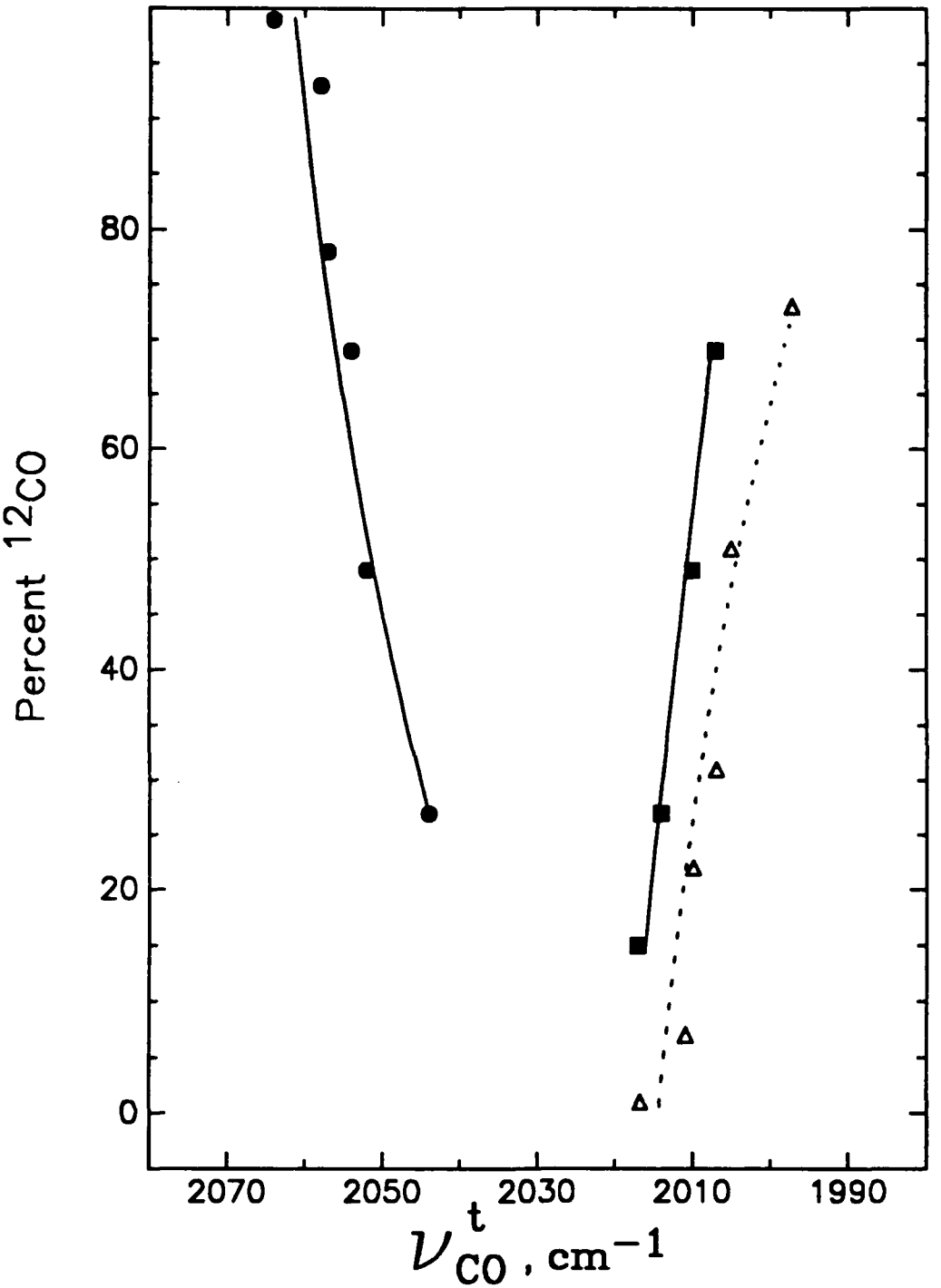

FIG 4

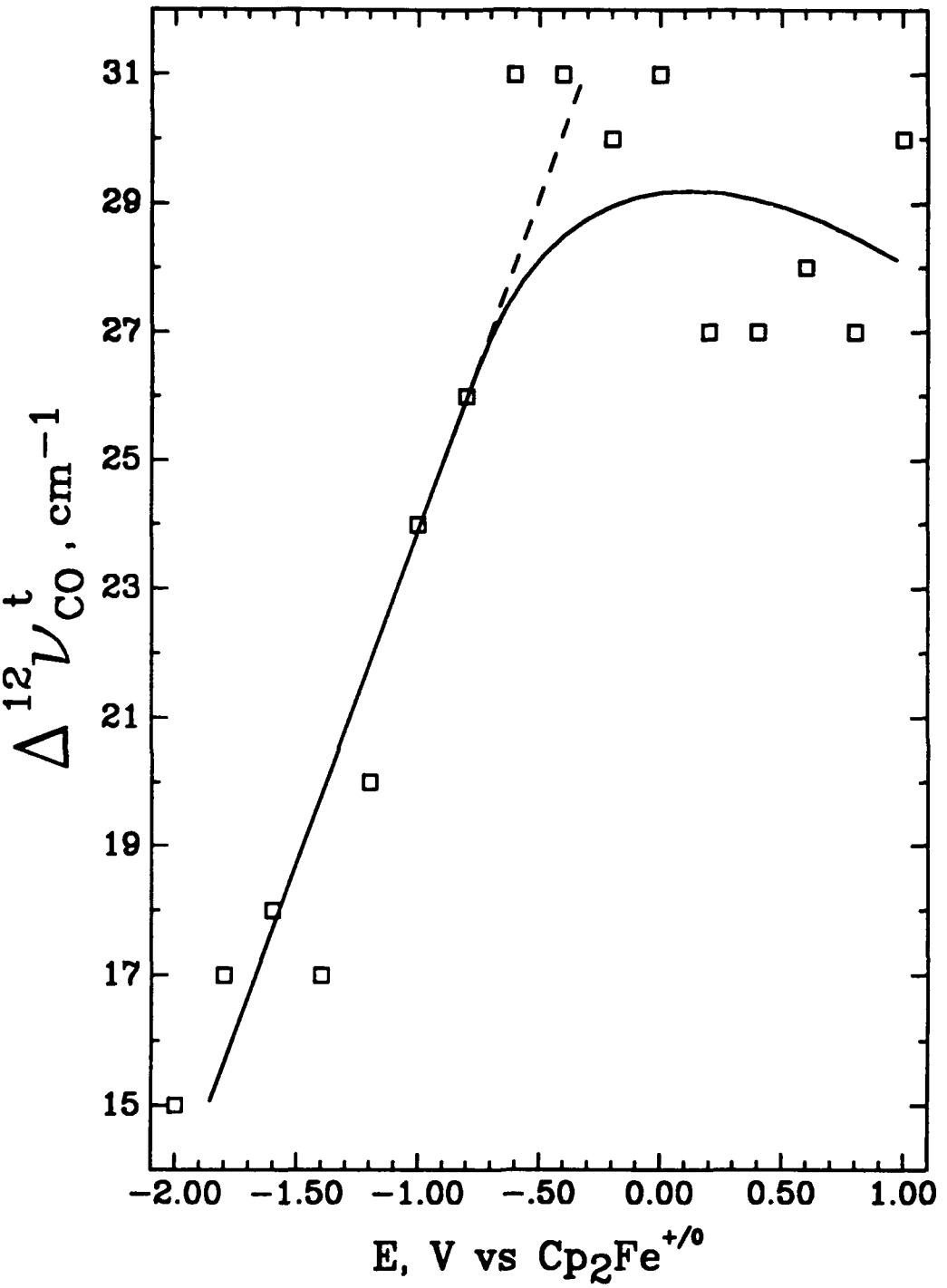
31
29
27
25
23
21
19
17
15
$\Delta^{12}\nu_{CO}{}^{t}$, cm^{-1}
−2.00
−1.50
−1.00
−.50
0.00
0.50
1.00
E, V vs $Cp_2Fe^{+/0}$

FIG 5

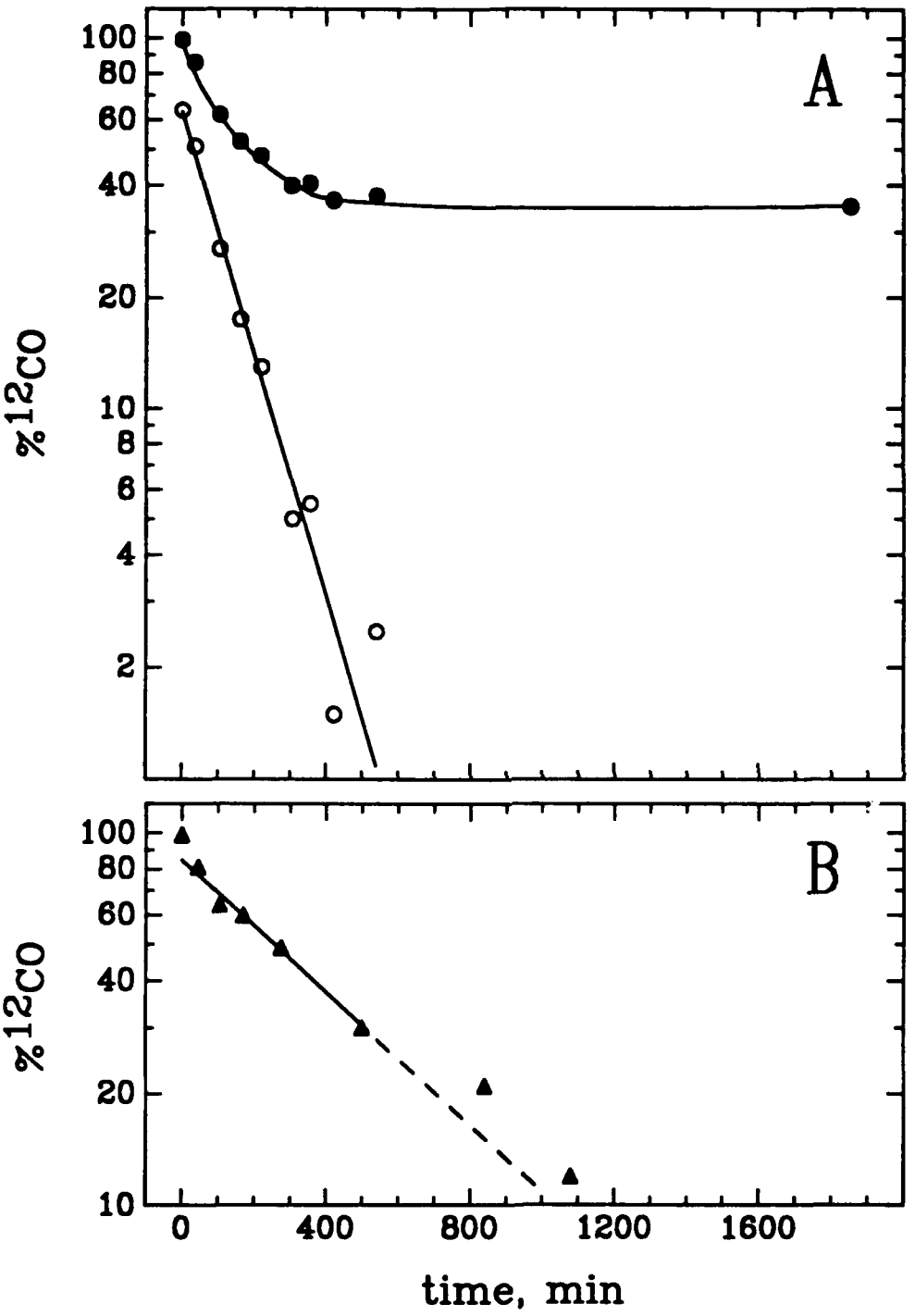

FIG 6

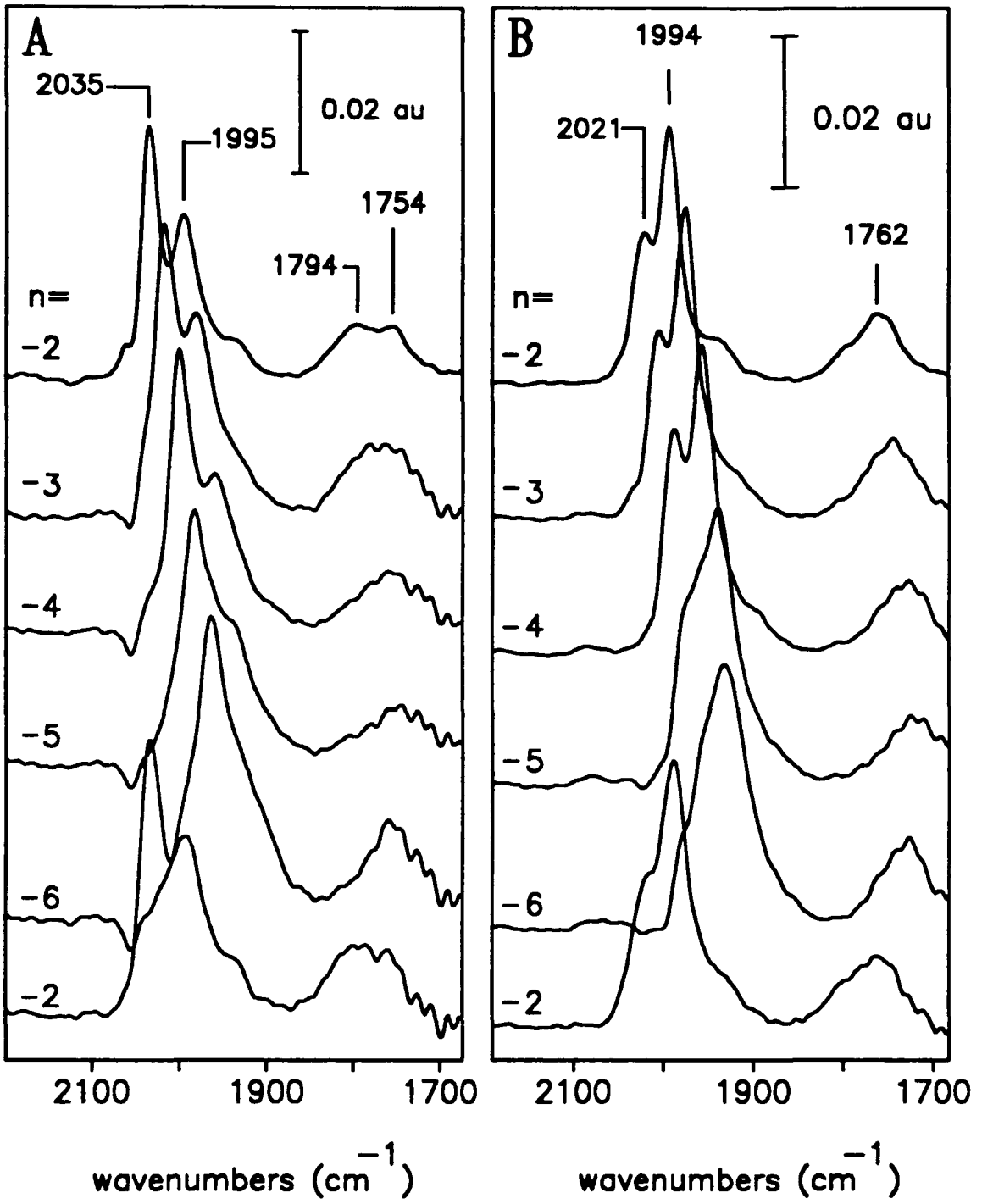
A
2035
1995
0.02 au
1754
1794
n=
-2
-3
-4
-5
-6
-2
2100
1900
1700
wavenumbers (cm^{-1})
B
1994
2021
0.02 au
1762
n=
-2
-3
-4
-5
-6
-2
2100
1900
1700
wavenumbers (cm^{-1})

FIG 7

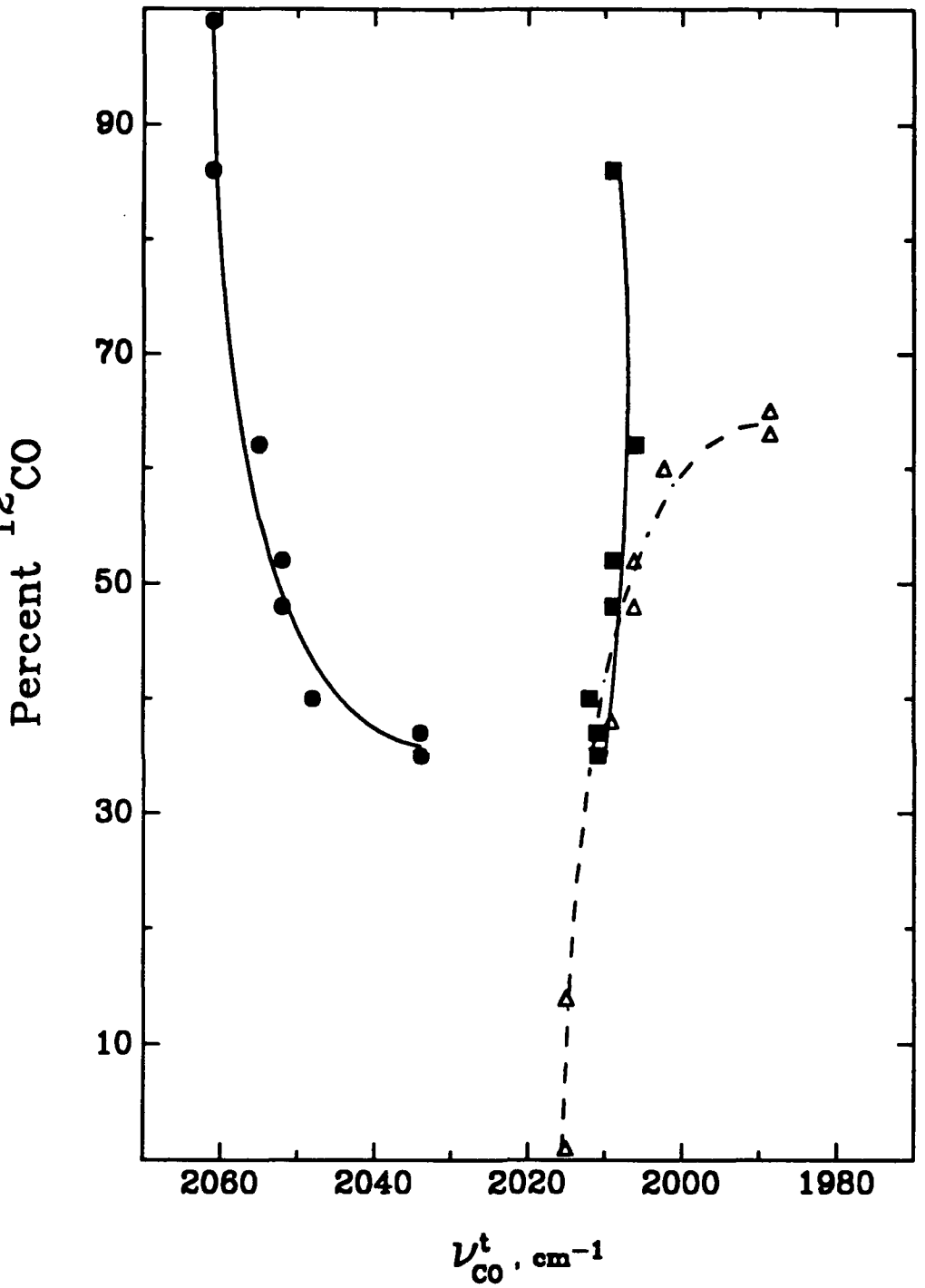

FIG 8

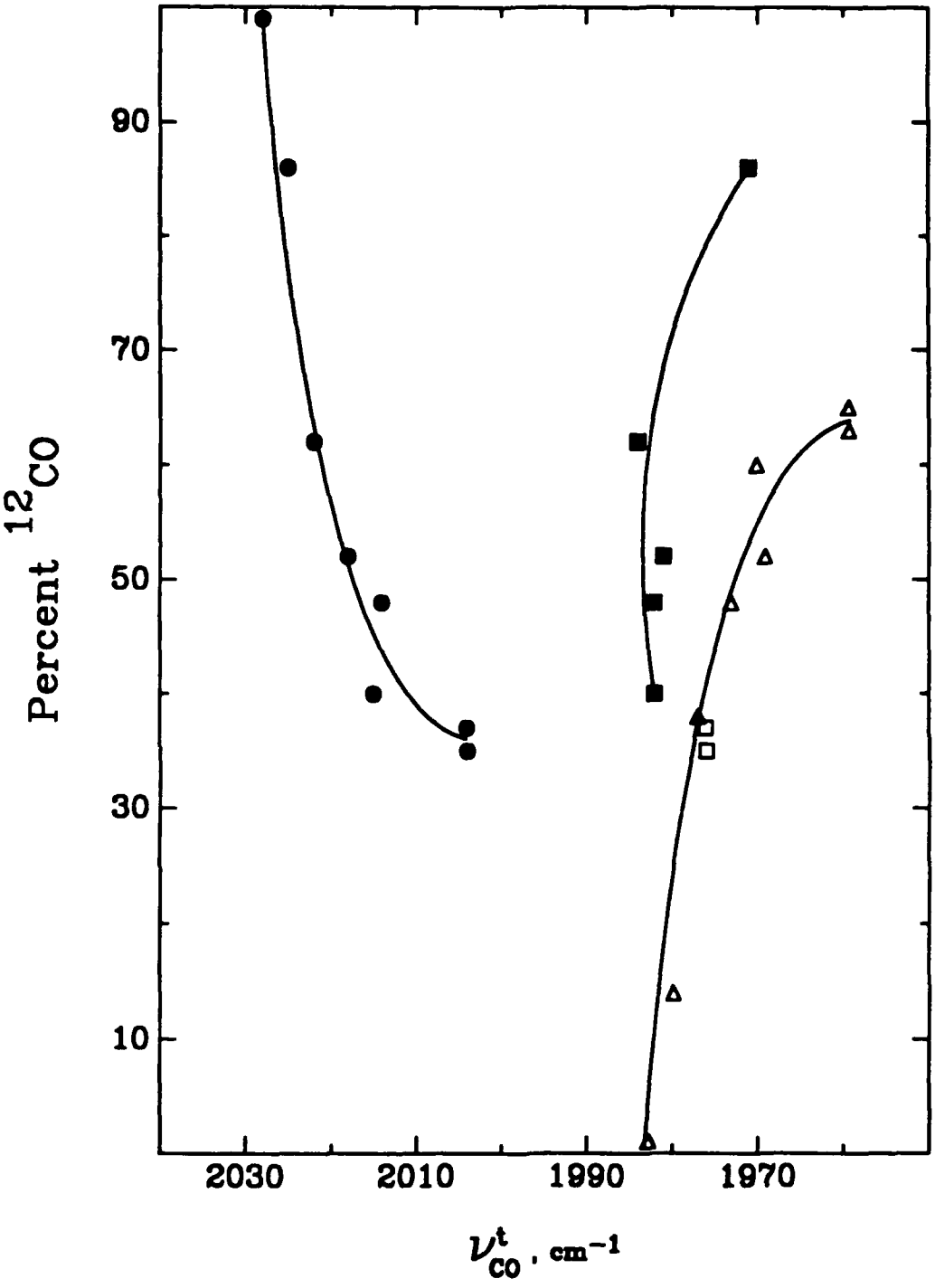

FIG 9

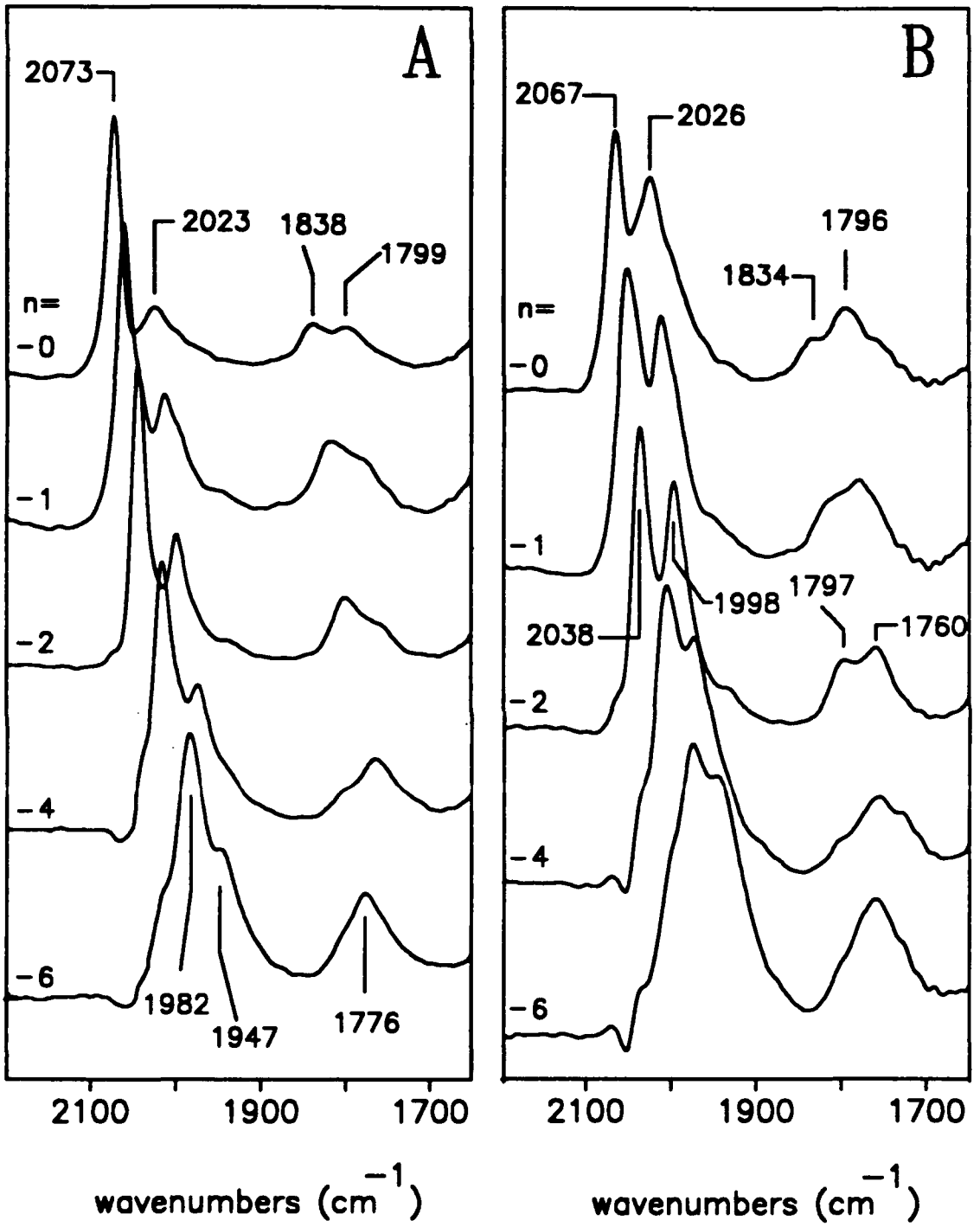
A
2073
2023
1838
1799
n=
-0
-1
-2
-4
-6
1982
1947
1776
2100
1900
1700
wavenumbers (cm^{-1})
B
2067
2026
1796
1834
n=
-0
-1
1998
1797
2038
1760
-2
-4
-6
2100
1900
1700
wavenumbers (cm^{-1})

FIG 10

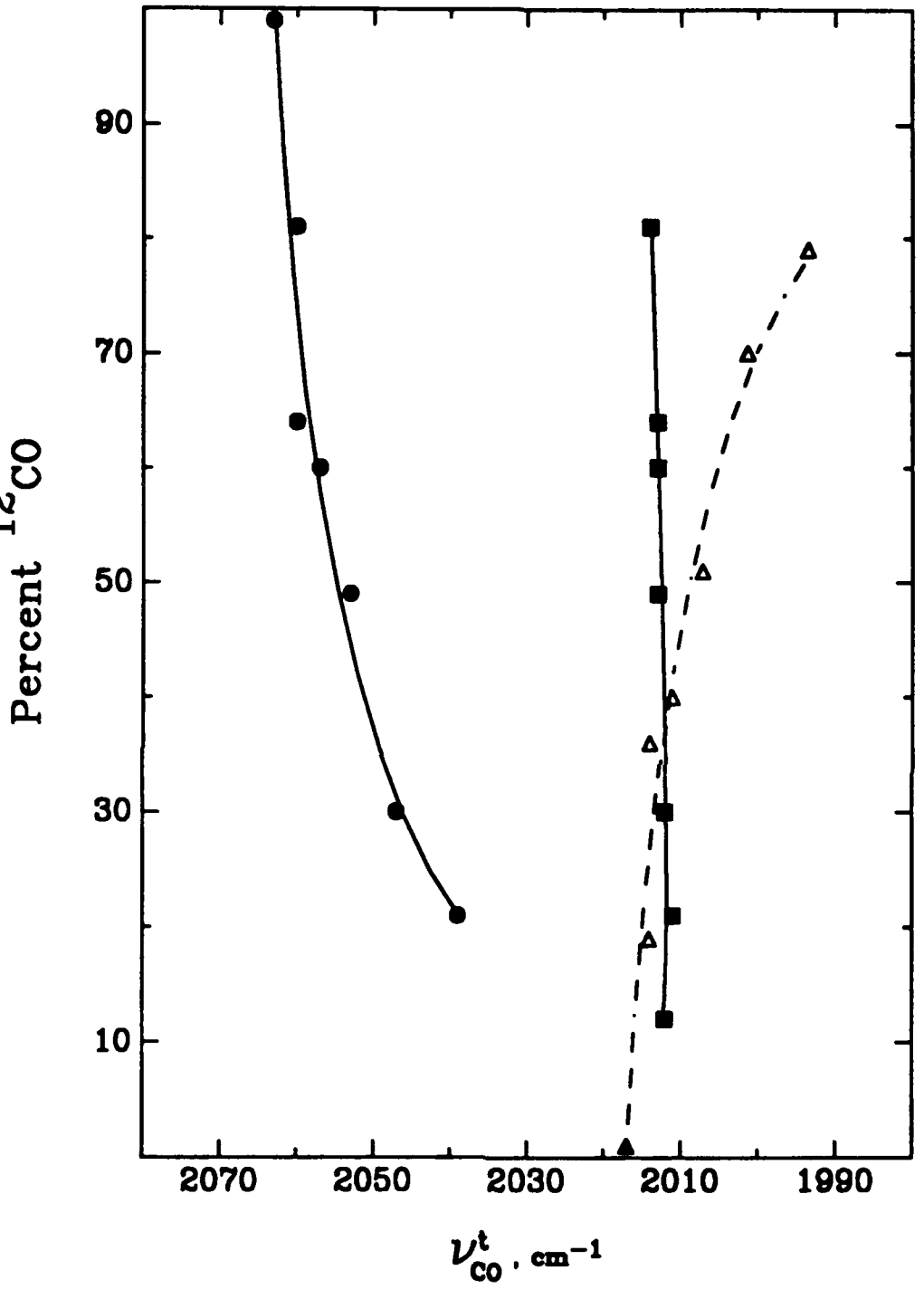

FIG 11

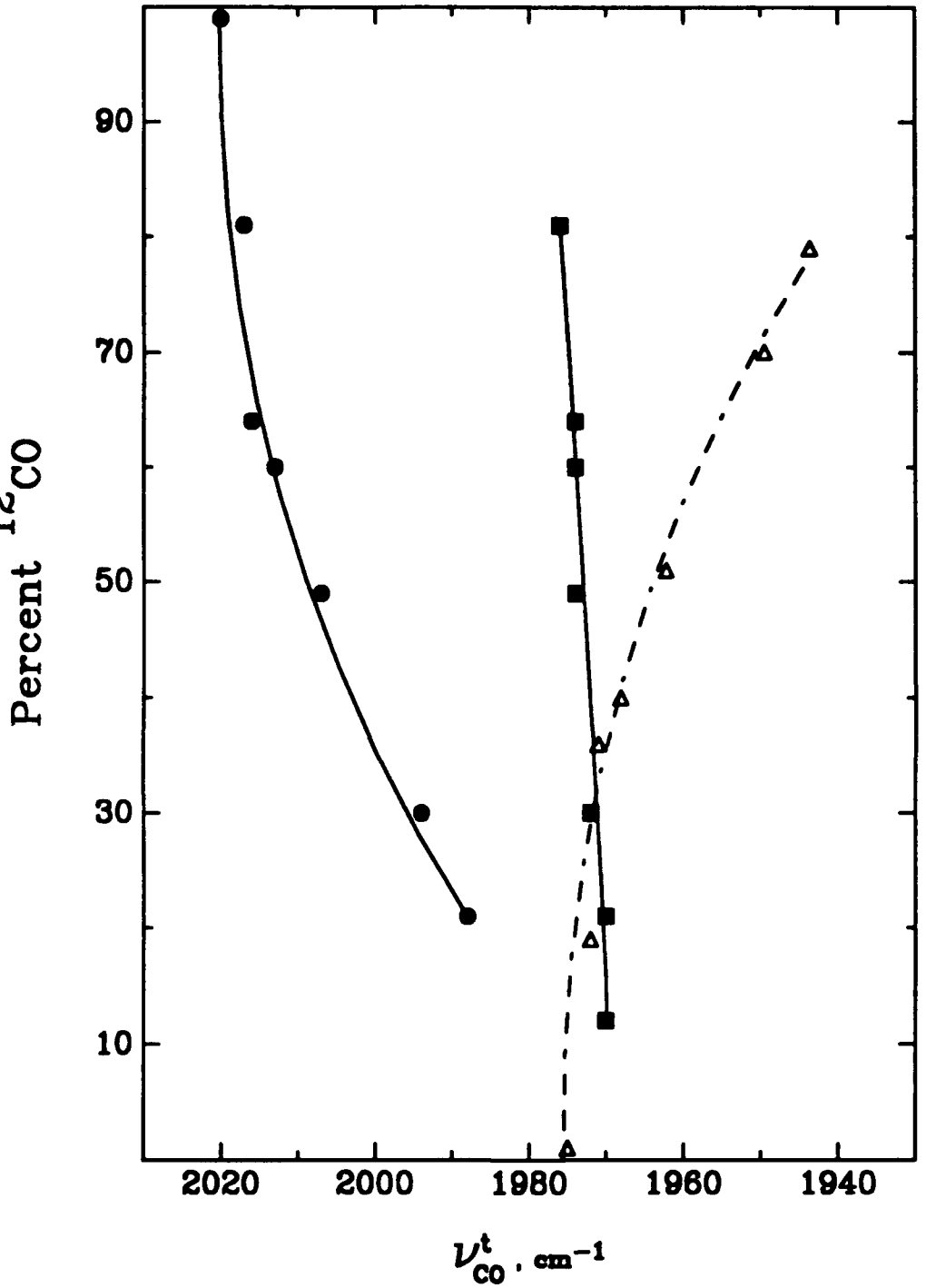

FIG 12

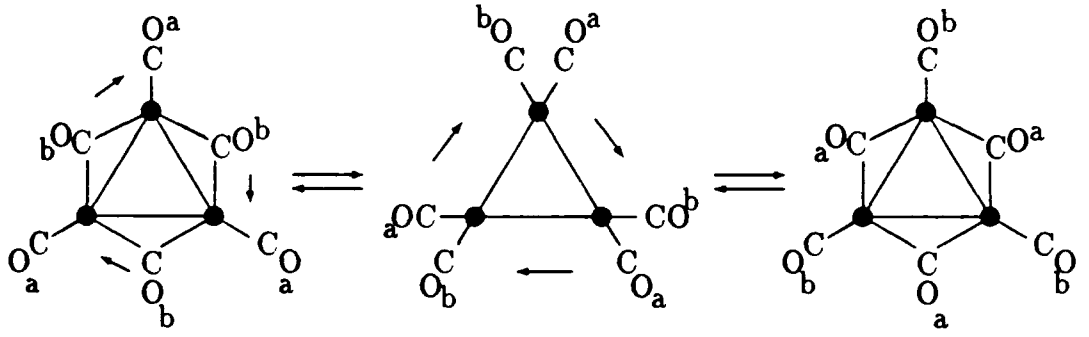

FIG 13

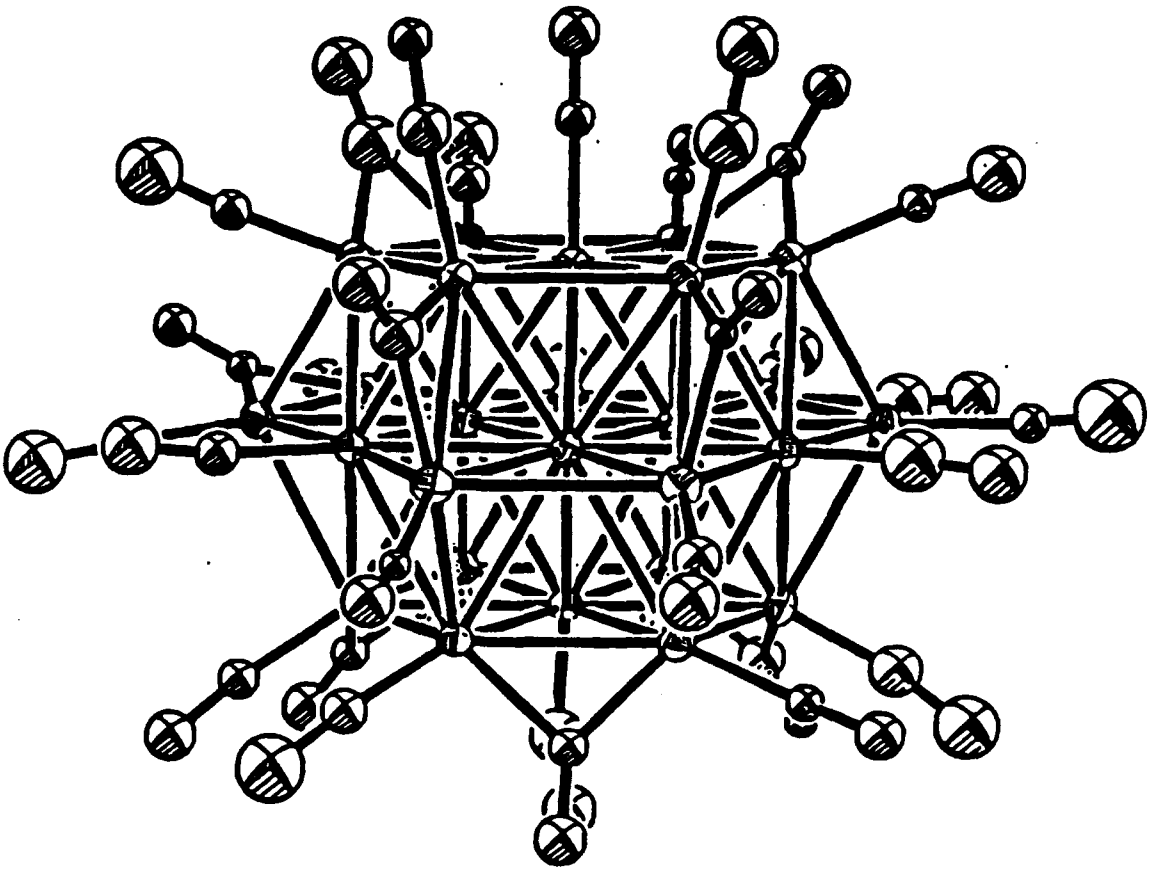

FIG 14

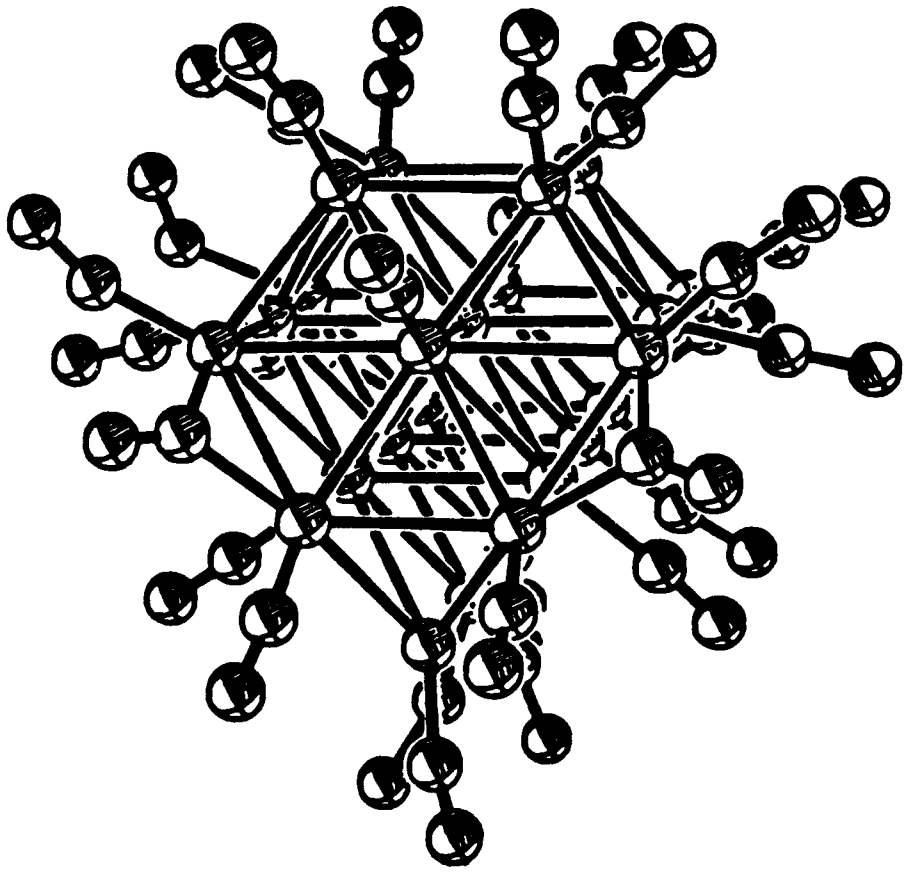

FIG 15